electronic reprint

Acta Crystallographica Section C
Crystal Structure Communications
ISSN 0108-2701
Editor: **George Ferguson**

$GdAlO_3$ perovskite

Douglas du Boulay, Nobuo Ishizawa and Edward (Ted) N. Maslen

Acta Crystallographica Section C
Crystal Structure Communications
ISSN 0108-2701

$GdAlO_3$ perovskite

Douglas du Boulay,[a] Nobuo Ishizawa[a]* and Edward (Ted) N. Maslen[b]‡

[a]Nagoya Institute of Technology, 10-6-29 Asahigaoka, Tajimi, Gifu 507-0071, Japan, and [b]Department of Physics, University of Western Australia, Nedlands 6009, WA, Australia
Correspondence e-mail: ishizawa@nitech.ac.jp

Received 10 August 2004
Accepted 5 October 2004
Online 23 November 2004

Flux-grown gadolinium aluminate perovskite, $GdAlO_3$, was examined using single-crystal 0.7 Å-wavelength synchrotron X-ray diffraction. In the context of other well categorized rare earth aluminate ($RAlO_3$) perovskite phases, the orthorhombic *Pnma* symmetry determined for the current compound is unsurprising. Corner-linked AlO_6 octahedra form the structural backbone of $RAlO_3$ perovskites and distort to accommodate the various rare earth ions in the structural voids. For $GdAlO_3$, the octahedral distortion, characterized by tilting of the octahedra about the shortest R—Al—R vectors, and octahedral deformation, characterized by strain of the octahedra along those axes, are in accordance with trends in the $RAlO_3$ series.

Comment

Rare earth perovskite oxides (RMO_3; R = Y, La– Lu, and M is a metal) have drawn scientific interest for many decades (*e.g.* Geller & Bala, 1956) and found applications as laser hosts (Li *et al.*, 1990), in recording media, in a variety of sensing applications and as high-temperature superconductors in the perovskite-like cuprates. Members of the $RFeO_3$ (Rearick *et al.*, 1993), RVO_3 (Miyasaka *et al.*, 2003), $RMnO_3$ (Ramirez, 1997), $RNiO_3$ (Piamonteze *et al.*, 2002), $RCoO_3$ (Samoilov *et al.*, 1998) and $RGaO_3$ (Ishihara *et al.*, 1998) series display wide ranges of interesting magnetic and conduction properties. In contrast, the rare earth aluminate perovskites ($RAlO_3$) are relatively less promising in these areas. Precise knowledge of their structural trends could, however, provide useful background information for resolving structural and electronic relationships in their technologically more important analogues.

The perovskite oxides are composed of relatively robust corner-linked M-centred MO_6 octahedra, with nominally 12-coordinated rare earth (R) cations. Most rare earth perovskites adopt low-symmetry distortions from the ideal cubic perovskite $Pm\bar{3}m$ symmetry. This is widely attributed to the cation size mismatch effect, whereby small radii R cations induce structural collapse through mechanisms involving tilting of rigid octahedra, small octahedral deformations and cation displacements (Glazer, 1972; Howard & Stokes, 1998; Woodward, 1997; Thomas, 1996, 1998).

As the atomic number (Z) increases across the periodic table from La to Lu, the 4*f* electron shell is filled and the mean atomic radius decreases. This lanthanide contraction is associated with structural distortions of increasing magnitude in rare earth perovskites (Geller & Bala, 1956; Dernier & Maines, 1971). Whereas $LaAlO_3$ is reportedly ideal cubic at 720 K (Geller & Bala, 1956), the symmetry reduces to $R\bar{3}c$ at room temperature, with rhombohedral distortions increasing from La to Nd. Between Nd and Sm, the stable room-temperature phase shifts in favour of orthorhombic *Pnma* symmetry (Marezio *et al.*, 1972), the most common low-symmetry perovskite distortion. According to the *Pnma* symmetry model, the M atoms are located on inversion centres, the R atom and atom O1 lie on the $y = \frac{1}{4}$ and $y = \frac{3}{4}$ mirror planes perpendicular to the orthorhombic b axis, and atom O2 occupies a site of general symmetry. Higher Z members of the $RAlO_3$ series are all isomorphous with the Sm member, and the lightest rare earth analogue, $YAlO_3$, has structural distortions comparable to those of $HoAlO_3$ (Geller & Wood, 1956; Diehl & Brandt, 1975).

Fig. 1 shows an AlO_6 octahedron of $GdAlO_3$ coupled to the shortest and therefore strongest Gd—O bonds in the lattice. The six short Gd—O bonds act on each octahedral vertex in a coherent manner, collectively leading to static tilting of the AlO_6 unit through an angle of 14.3°, acting about a pseudo-threefold axis closely aligned with the shortest collinear Gd—Al—Gd contacts in the structure. This suggests that a model of the lattice in terms of linked Gd-bicapped octahedra, as shown in Fig. 2, could be as useful as the more customary representation in terms of corner-linked octahedra. Tilt angles of 5.8, 6.5, 9.5, 12.2 and 16.9° have been observed for La, Pr, Nd,

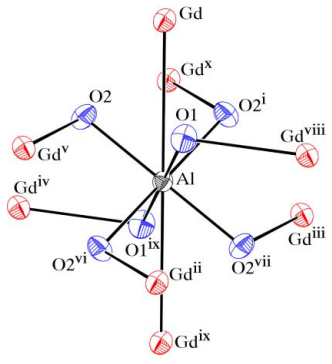

Figure 1
Pseudo-threefold symmetry of the AlO_6 octahedra in $GdAlO_3$. Foreshortened Gd—O1 [2.3069 (7) Å] and Gd—O2 [2.3391 (5) Å] bonds (all symmetry combinations) induce static tilting of the octahedra about a Gd—Al—Gd^{ix} [2 × 3.0793 (3) Å] axis. [Symmetry codes: (i) $\frac{1}{2} - x, -y, \frac{1}{2} + z$; (ii) $-1 + x, y, z$; (iii) $\frac{1}{2} - x, -\frac{1}{2} + y, \frac{1}{2} + z$; (iv) $\frac{1}{2} - x, -y, -\frac{1}{2} + z$; (v) $-\frac{1}{2} + x, \frac{1}{2} - y, \frac{3}{2} - z$; (vi) $-\frac{1}{2} + x, y, \frac{3}{2} - z$; (vii) $-x, -y, 2 - z$; (viii) $-\frac{1}{2} + x, \frac{1}{2} - y, \frac{5}{2} - z$; (ix) $-x, -\frac{1}{2} + y, 2 - z$; (x) $1 - x, -\frac{1}{2} + y, 2 - z$.]

‡ Deceased 2 February 1997.

  DOI: 10.1107/S0108270104025144

Sm and Ho aluminate perovskites, respectively (du Boulay, 1997).

Megaw & Darlington (1975) characterized octahedral deformation in rhombohedrally distorted perovskites in terms of the octahedron strain, ζ, describing flattening or elongation along a single preserved octahedral threefold axis. Specifically, $(1+\zeta) = c_{hex}/[2(6)^{1/2}\,\bar{l}_{\perp}]$, where c_{hex} is the hexagonal c-axis length and $\bar{l}_{\perp}$ is the mean length of the six octahedral O$\cdots$O contact edges oriented normal to that threefold axis.

The pseudo-threefold axes of the Gd-bicapped octahedra shown in Fig. 2 suggest that an equivalent parameterization of octahedral strain in orthorhombically distorted octahedra may be relevant. Although there are four approximate threefold axes, only the bicapping axis identified in Figs. 1 and 2 demonstrates marked structural continuity across the phase transition. Quantifying the strain along that axis involves a more intimate description in terms of the distance, h, separating the upper and lower triangular faces oriented normal to the pseudo-threefold axis, or $\bar{l}_{\parallel}$, the mean of the six O$\cdots$O contact lengths connecting those two faces. $(1+\zeta) = (3/2)^{1/2}(h/\bar{l}_{\perp}) = [3\bar{l}_{\parallel}{}^2/(2\bar{l}_{\perp}{}^2) - 1/2]^{1/2}$

For $GdAlO_3$, ζ has a value of 0.0012 (2), contrasting with values of −0.003, −0.014, −0.022, −0.004 and 0.012 for La, Pr, Nd, Sm and Ho, respectively (du Boulay, 1997). A discontinuity in the strain tendency between Nd and Sm suggests that alleviating the initial rapid increase in octahedral compression as the octahedral tilt angle increases smoothly across the series may be the prime motivating factor behind the rhombohedral to orthorhombic $RAlO_3$ phase change. This is not to say that strain is the fundamental order parameter, but presumably it correlates strongly with some pertinent attributes of the bonding and electronic configuration of the Al atom. The octahedron strain and tilt in $GdAlO_3$ itself place it comfortably within the orthorhombic perovskite distortion regime.

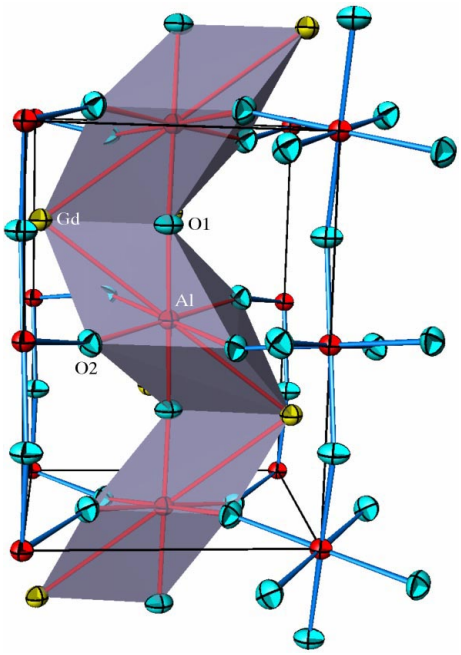

Figure 2
An *ATOMS* (Dowty, 2002) representation of the extended $GdAlO_3$ unit cell, demonstrating shared-edge connectivity between mirror-related Gd-bicapped octahedra.

Experimental

Crystals of $GdAlO_3$ were grown using the high-temperature flux growth technique of Wanklyn (1969), by dissolving Gd_2O_3 and Al_2O_3 in a PbO, PbF_2 and B_2O_3 flux. The mixture was heated rapidly to 1580 K in a 10 ml platinum crucible and then cooled slowly to 1280 K at 10 K h^{-1}. The crystals were liberated by dissolving the residual flux in hot dilute nitric acid. $GdAlO_3$ crystals were easily identified by their rectangular prismatic habit with pronounced (101), (10$\bar{1}$) and (010) faces.

Crystal data

$GdAlO_3$
M_r = 232.23
Orthorhombic, *Pnma*
a = 5.3049 (7) Å
b = 7.4485 (9) Å
c = 5.2537 (6) Å
V = 207.59 (4) Å^3
Z = 4
D_x = 7.43 Mg m^{-3}
Synchrotron radiation
λ = 0.7 Å
Cell parameters from 12 reflections
θ = 20–30°
μ = 29.65 mm^{-1}
T = 295 K
Rectangular prism, colourless
0.03 × 0.02 × 0.02 mm

Data collection

Rigaku BL14A four-circle diffractometer
$\omega/2\theta$ scans
Absorption correction: analytical (de Meulenaer & Tompa, 1965)
T_{min} = 0.412, T_{max} = 0.586
8547 measured reflections
1193 independent reflections
1193 reflections with $F > 0$
R_{int} = 0.034
θ_{max} = 50.0°
$h = -11 \rightarrow 11$
$k = -16 \rightarrow 16$
$l = -11 \rightarrow 11$
6 standard reflections
every 94 reflections
intensity decay: none

Refinement

Refinement on F
R = 0.012
wR = 0.009
S = 2.06
1193 reflections
29 parameters
$w = 1/[\sigma^2(F_o)]$
$(\Delta/\sigma)_{max}$ = 0.001
$\Delta\rho_{max}$ = 1.25 e Å^{-3}
$\Delta\rho_{min}$ = −3.68 e Å^{-3}
Extinction correction: Zachariasen (1968)
Extinction coefficient: 9780 (173)

Measured structure factors were optimized against calculated structure factors derived from neutral atomic form factors combined with the wavelength-dependent dispersion corrections of Sasaki (1989). Least-squares agreement indices $wR(F)$ support the notion of this as a high-precision diffraction experiment. Modest electron-density differences were encountered. The largest of these were two independent depletions, −3.7 (2) and −3.3 (2) e Å^{-3} in magnitude, both located 0.4 Å from the Gd atom and diametrically disposed. They maximize within the mirror plane normal to [010] and their respective Gd vectors were directed along [100], normal to the shortest Gd—O1 bonds.

Data collection: *DIFF*14*A* (Satow & Iitaka, 1989); cell refinement: *DIFF*14*A*; data reduction: *DIFDAT*, *ADDREF*, *SORTRF* and *ABSORB* in *Xtal*3.7.2 (Hall *et al.*, 2003); program(s) used to solve structure: *Xtal*3.7.2; program(s) used to refine structure: *CRYLSQ* in *Xtal*3.7.2; molecular graphics: *Xtal*3.7.2 and *ATOMS* (Dowty, 2002); software used to prepare material for publication: *BONDLA* and *CIFIO* in *Xtal*3.7.2.

The authors thank Dr N. R. Streltsova for providing the crystal. These studies were conducted while DduB was supported by a postgraduate scholarship from the Special

Research Centre for Applied Materials and Minerals Processing (SRCAMMP) at the University of Western Australia. The late ENM's expertise and devoted tutelage were greatly appreciated by DduB during that period, and ENM remains sadly missed.

Supplementary data for this paper are available from the IUCr electronic archives (Reference: SQ1172). Services for accessing these data are described at the back of the journal.

References

Boulay, D. du (1997). PhD thesis, University of Western Australia, Australia.
Dernier, P. D. & Maines, R. G. (1971). *Mater. Res. Bull.* **6**, 433–440.
Diehl, R. & Brandt, G. (1975). *Mater. Res. Bull.* **10**, 85–90.
Dowty E. (2002). *ATOMS*. Version 6.1. Shape Software, 521 Hidden Valley Road, Kingsport, TN 37663, USA.
Geller, S. & Bala, V. B. (1956). *Acta Cryst.* **9**, 1019–1025.
Geller, S. & Wood, E. A. (1956). *Acta Cryst.* **9**, 563–568.
Glazer, A. M. (1972). *Acta Cryst.* B**28**, 3384–3392.
Hall, S. R., du Boulay, D. J. & Olthof-Hazekamp, R. (2003). Editors. *Gnu Xtal*3.7.2 *System*. University of Western Australia, Australia. (URL: http://xtal.sourceforge.net/.)
Howard, C. J. & Stokes, H. T. (1998). *Acta Cryst.* B**54**, 782–789.
Ishihara, T., Honda, M., Shibayama, T., Minami, H., Nishiguchi, H. & Takita, J. (1998). *Electrochem. Soc.* **145**, 3177–3183.
Li, G., Shi, Z., Guo, X., Wu, J., Chen, Y. & Chen, J. (1990). *J. Cryst. Growth*, **106**, 524–530.
Marezio, M., Dernier, P. D. & Remeika, J. P. (1972). *J. Solid State Chem.* **4**, 11–19.
Megaw, H. D. & Darlington, C. N. W. (1975). *Acta Cryst.* A**31**, 161–173.
Meulenaer, J. de & Tompa, H. (1965). *Acta Cryst.* **19**, 1014–1018.
Miyasaka, S., Okimoto, Y., Iwama, M. & Tokura, Y. (2003). *Phys. Rev. B*, **68**, R100406–R100409.
Piamonteze, C., Tolentino, H. C. N., Ramos, A. Y., Massa, N. E., Alonso, J. A., Martinez-Lope, M. J. & Casais, M. T. (2002). *Physica B*, **320**, 71–74.
Ramirez, A. P. (1997). *J. Phys. Condens. Matter*, **9**, 8171–8199.
Rearick, T. M., Catchen, G. L. & Adams, J. M. (1993). *Phys. Rev. B*, **48**, 224–238.
Samoilov, A. V., Beach, G., Fu, C. C., Yeh, N.-C. & Vasquez, R. P. (1998). *Phys. Rev. B*, **57**, R14032–R14035.
Sasaki, S. (1989). KEK Report 88-14, pp. 5–35. National Laboratory for High Energy Physics, Tsukuba, Japan.
Satow, Y. & Iitaka, Y. (1989). *Rev. Sci. Instrum.* **60**, 2390–2393.
Thomas, N. W. (1996). *Acta Cryst.* B**52**, 954–960.
Thomas, N. W. (1998). *Acta Cryst.* B**54**, 585–599.
Wanklyn, B. M. (1969). *J. Cryst. Growth*, **5**, 323–328.
Woodward, P. M. (1997). *Acta Cryst.* B**53**, 32–43.
Zachariasen, W. H. (1968). *Acta Cryst.* A**24**, 212–216.